

Toward Strong Interactions in Circular Quantum Dots: Correlation Induced Inhomogeneity

Amit Ghosal,¹ A. D. Güçlü,² C. J. Umrigar,² Denis Ullmo,^{1,3} and Harold U. Baranger¹

¹*Department of Physics, Duke University, Durham, North Carolina 27708-0305*

²*Theory Center and Laboratory of Atomic and Solid State Physics, Cornell University, Ithaca, New York 14853*

³*Laboratoire de Physique Théorique et Modèles Statistiques (LPTMS), 91405 Orsay Cedex, France*

PACS numbers: 73.23.Hk, 73.63.Kv, 02.70.Ss

Physical properties of the “electron gas” – in which conduction electrons interact via Coulomb forces but the ionic potential is neglected – change dramatically depending on the balance between the strength of the kinetic energy and the Coulomb repulsion. The limiting cases are well understood¹: For weak interactions (high density), the system behaves as a Fermi liquid, with delocalized electrons. In contrast, in the strongly interacting limit (low density), the electrons localize and become ordered in a Wigner crystal phase. The physics at intermediate densities is phenomenally rich and remains a subject of fundamental research.^{2,3,4,5} Here we study the intermediate density electron gas confined to a circular quantum dot. By using accurate quantum Monte Carlo techniques,⁶ we show that the correlation induced by increasing interaction strength smoothly causes, first, ring structure and, then, angular modulation, without any signature of a sharp transition or even a cross-over in this density regime.

Quantum dots⁷ – a nanoscale island containing a puddle of electrons – provide a highly tunable and simple setting to study the effects of large Coulomb interaction. They introduce level quantization and quantum interference in a controlled way. As one can in principle make them in the very low density regime for which correlation effects are strong,⁸ it is only a matter of time before such dots are studied experimentally.

We therefore consider a model quantum dot consisting of electrons moving in a two dimensional (2D) plane, with kinetic energy $(-\frac{1}{2}\sum_i \nabla_i^2)$, and interacting with each other by long-range Coulomb repulsion $(\sum_{i<j} |\mathbf{r}_i - \mathbf{r}_j|^{-1})$. All energies are expressed in atomic units, defined by $\hbar = e^2/\epsilon = m^* = 1$ (with electronic charge e , effective mass m^* , and dielectric constant ϵ). The electrons are confined by an external quadratic potential $V_{\text{ext}}(\mathbf{r}) = \frac{1}{2}\omega^2 r^2$. The spring constant ω controls the density and is varied between 3.0 and 0.0075. The ratio between the strength of the Coulomb interaction and the kinetic energy is usually characterized by the interaction parameter $r_s \equiv (\pi n)^{-1/2}$, with n the density of electrons. For our confined system in which $n(\mathbf{r})$ varies, we define r_s in the same way using the mean density $\bar{n} \equiv \int n^2(\mathbf{r}) d\mathbf{r}/N$. We have studied this system with up to $N = 20$ electrons; for the range of ω considered, r_s is between 0.4 and 17.7.

In the bulk 2D electron gas, numerical work suggests a direct phase transition between the Fermi liquid and Wigner crystal states in two dimensions² with a critical $r_s^c \approx 37$. On the other hand, experiments (which include, of course, disorder and residual effects of the ions) on the 2D electron gas observe more complex behavior, including evidence for a metal-

insulator transition.^{4,5}

Circular quantum dots have been studied previously using a variety of methods, yielding a surprisingly inconclusive scenario. Many studies have used mean field methods^{9,10,11} such as density functional theory or Hartree-Fock. These typically predict charge or spin density wave order even for modest r_s (unless the symmetry is restored after the fact – see Ref.11) which raises questions about their accuracy. Exact diagonalization calculations^{12,13} are free of the mean-field approximation but are restricted to small N and r_s . Path integral quantum Monte Carlo (PIMC) has also been applied: One study¹⁴ found a crossover from Fermi liquid to “Wigner molecule” at a single $r_s \approx 4$ – a value significantly smaller than the 2D bulk r_s^c . Another,¹⁵ using different criteria, found a two-stage transition for r_s significantly larger than r_s^c . Although PIMC treats interactions accurately, it has its own systematic and statistical problems: it becomes inefficient as $T \rightarrow 0$ and it generates a thermal average of states with different L and S quantum numbers, preserving only S_z symmetry.

To avoid these various difficulties and so clarify the scenario, we have carried out a study using the variational and diffusion Monte Carlo techniques,⁶ which we used previously to study both circular^{16,17} and irregular¹⁸ dots at $r_s \sim 2$. This method is free of the problems of PIMC but is approximate in that a “fixed-node” error is made. We believe the latter is small for the range of parameters studied here, as described in the “methods” section below. Using well optimized trial wave functions, the statistical and systematic errors of DMC are much smaller than the statistical errors of the published PIMC results; a detailed comparison to PIMC and exact diagonalization results is presented in the supplementary material.

Results for the electron density, $n(\mathbf{r})$, are shown in Fig. 1. There is a dramatic change in $n(\mathbf{r})$ upon increasing interaction strength: For weak interactions [panel (a)], the density is rather homogeneous; the small modulation seen is caused by shell effects in the orbitals of the mean-field problem. In contrast, large r_s induces strong radial modulation in $n(\mathbf{r})$ [panel (b)], resulting in the formation of rings. Because the ground state has $L = 0$ (this is a closed shell configuration in the non-interacting limit), no angular modulation of the density can occur. Interestingly, for $r_s > 10$ the number of rings for each N is the same as that seen in the classical limit^{19,20} ($r_s \rightarrow \infty$), e.g. three rings for $N = 20$.

We find that the formation of rings and the increase in their sharpness is very smooth, without any sign of a threshold. This is shown quantitatively in Fig. 1(d) by using the fractional peak height (FPH, defined in Fig. 1(c)) of the outer ring

arXiv:cond-mat/0601178 v2 16 Jan 2006

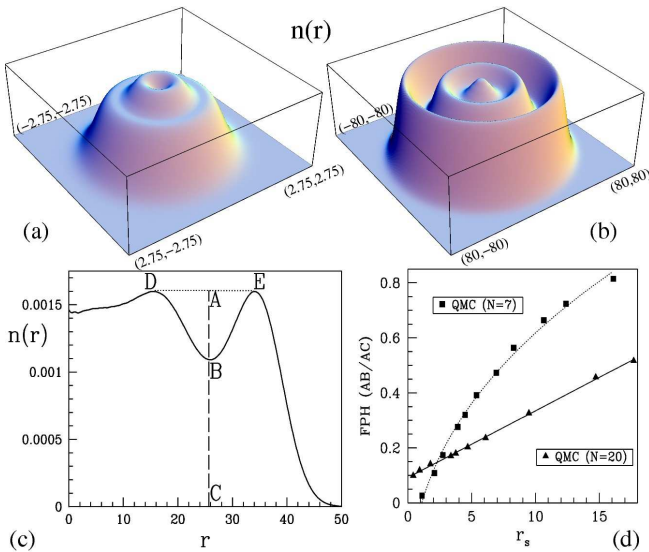


FIG. 1: Electron density, $n(\mathbf{r})$, for the ground state of a $N = 20$ circular quantum dot ($L = 0, S = 0$). The extrapolated quantum Monte Carlo (QMC) estimator is used.⁶ (a) High density: $r_s \approx 0.4$ ($\omega = 3.0$). (b) Low density: $r_s \approx 15$ ($\omega = 0.01$). Note the dramatic change in electron density upon decreasing the density: the electron-electron correlation caused by stronger interactions at low density produces sharp rings. The 3 ring structure agrees with that seen in the classical limit. (c) Radial cut of $n(\mathbf{r})$ for $r_s \approx 10$ ($\omega = 0.02$) where the 3-ring structure is about to appear. The degree of modulation is quantitatively characterized by the fractional peak height (FPH): draw the line tangential to the outer two peaks of $n(\mathbf{r})$ (\overline{DE}), then find the vertical line \overline{AC} along which the distance from \overline{DE} to $n(\mathbf{r})$ is maximum, and finally define the FPH as the ratio of the two lengths $\overline{AB}/\overline{AC}$. (d) FPH as a function of r_s for $N = 20$ and 7. The evolution of FPH for $N = 20$ is linear and completely featureless for $r_s \lesssim 18$. The solid line is a linear fit to the data. For smaller N , radial modulation in $n(\mathbf{r})$ becomes stronger, leading to $FPH \rightarrow 1$ for large r_s , and a deviation from linearity occurs (the dotted line $\sim r_s^{0.41}$ is the best fit for $N = 7$). For our largest r_s , FPH typically grows with decreasing N , though not always monotonically. For example, it is largest for $N = 7$, which yields a ‘perfect crystal’ with equidistant electrons and thus produces a peak in the addition energy (See Fig 3a). The Monte Carlo statistical error is less than the size of the points.

to characterize the degree of ring structure. The resulting curve for FPH as a function of r_s is *smooth* – no deviations or special value of r_s can be seen.

Having established the formation of radial rings as a result of strong correlations, we turn to angular modulation – the issue of correlation induced localization of the individual electrons in each of the circular rings. In all the cases we consider, the density $n(\mathbf{r})$ is circularly symmetric, as is the density of spin up and down electrons separately, as required in two-dimensional systems, since we work with states of definite angular momentum L . We therefore consider the pair-densities $g_{\uparrow\downarrow}(\mathbf{r}_0; \mathbf{r})$, $g_{\uparrow\uparrow}(\mathbf{r}_0; \mathbf{r})$, and $g_T(\mathbf{r}_0; \mathbf{r})$, where $g_{\sigma\sigma'}(\mathbf{r}_0; \mathbf{r})$ is the probability of finding an electron with spin σ' at location \mathbf{r} when an electron with spin σ is held fixed at \mathbf{r}_0 and $g_T = g_{\uparrow\uparrow} + g_{\uparrow\downarrow}$. $g_{\sigma\sigma'}$ detects, in addition to the formation of radial

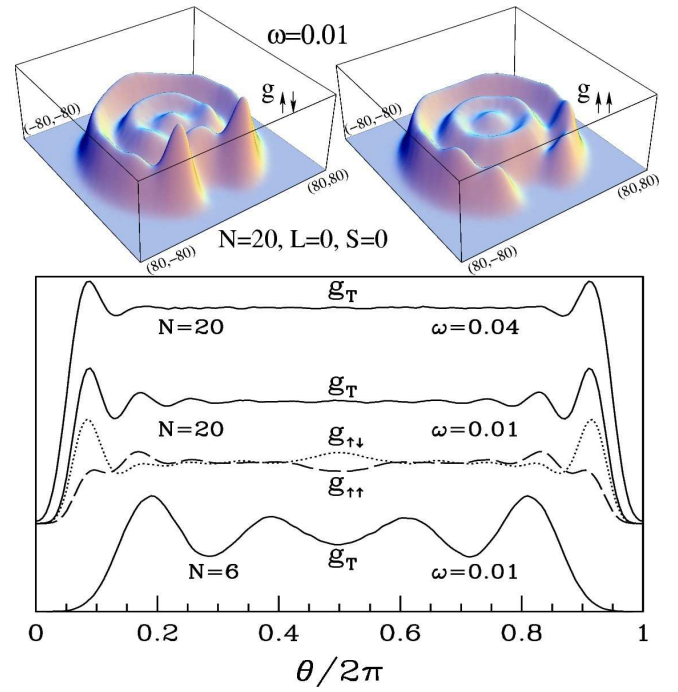


FIG. 2: Pair density of the circular quantum dot with an up-electron fixed on the outer ring. Top: $g_{\uparrow\downarrow}(\mathbf{r}_0; \mathbf{r})$ (left) and $g_{\uparrow\uparrow}(\mathbf{r}_0; \mathbf{r})$ (right) for the $N = 20$ ground state ($L = 0, S = 0$) with $r_s \approx 15$ ($\omega = 0.01$, $\mathbf{r}_0 = (57, 0)$). Short-range order develops near the fixed electron, indicating ‘incipient’ Wigner localization but not true long-range order. Bottom: Evolution of angular oscillations along the outer ring with r_s and N . The top trace shows $0.65 \times g_T$ for $r_s \approx 6$, $N = 20$: though strong radial modulation has already appeared, leading to ‘ring formation’, there is almost no angular modulation. The middle trace is g_T for $r_s \approx 15$, $N = 20$: clear angular structure is present, though compared to the ring modulation it is weak and short-range. Spin-resolved angular structure is also shown here; note the peculiar bump at $\theta = \pi$. The bottom trace is g_T for $r_s \approx 16$, $N = 6$ ($L = 0, S = 0$): for small N , angular modulation is clearly stronger. (The y-axis is shifted and scaled for $N = 20$ for clarity.)

rings, any angular structure induced by the interactions.

The most prominent feature in the pair density is a hole around the location of the fixed electron. For unlike spins, it is caused purely by Coulomb repulsion (correlation hole), while for like spins the antisymmetry of the wave function plays an important role (exchange hole). For small r_s , correlation is weak, so the hole in $g_{\sigma, -\sigma}$ is much smaller than that in $g_{\sigma, \sigma}$. As r_s increases, the correlation hole grows bigger, becoming of the same size as the exchange hole around $r_s \approx 4-5$.

Results for the pair density in the circular quantum dot are shown in Fig. 2 for an up-electron fixed on the outer ring. For $N = 20$ at large r_s , there are clear oscillations along the angular direction near \mathbf{r}_0 . This signals ‘incipient’ Wigner localization. However, these oscillations are weak (much weaker than the radial modulation) and short-ranged (damped), indicating that true long-range order is not yet established. As for radial modulation, the amplitude of the angular oscillations grows continuously, without any threshold value.

The evolution of the angular oscillations as a function of r_s

and N is illustrated in the bottom panel of Fig. 2. Comparing the top two traces, for $r_s \approx 6$ and 15 at $N = 20$, we see that g_T is almost featureless even for an r_s substantially bigger than 1, while short-range oscillations have set in by our larger r_s . The weakness of these oscillations suggests that electrons remain more or less delocalized along the ring for $N = 20$ up to the largest r_s studied. An intriguing feature of the spin-resolved pair densities shown is the bump at $\theta = \pi$: $g_{\uparrow\uparrow}$ decreases while $g_{\uparrow\downarrow}$ increases compared to the average value. This feature is present for all $r_s \geq 4$ and tends to grow with increasing interaction strength; we have no explanation for it at this time. Turning now to smaller N , we find that two rings are present for $N = 6$ at large r_s : the outer one has 5 electrons while the remaining electron is at the center. The lower trace in Fig. 2 shows that individual electrons are better localized for small N , a behavior that we find holds quite generally.

We next turn our attention to the addition energy, $\Delta^2 E(N) = E_G(N+1) + E_G(N-1) - 2E_G(N)$. This is experimentally accessible as the spacing between conductance peaks in a Coulomb blockade transport measurement, and is given by the charging energy in the simplest model of a quantum dot.⁷ Our results for $\Delta^2 E(N)$ (normalized by ω) for different interaction strengths are shown in Fig. 3 (r_s for fixed ω varies slightly with N). For $r_s \approx 2$, $\Delta^2 E(N)$ is similar to previous studies^{9,16} and consistent with weakly interacting physics: non-interacting “shell effects” produce strong peaks for closed shell configurations ($N = 6, 12, 20$). At larger r_s , the peaks weaken considerably, reducing mesoscopic fluctuations in $\Delta^2 E$. For similar r_s , shell effects are more strongly affected for small N , while their remnant persists for large N . For comparison, we plot the addition energy in the classical limit^{19,20} obtained from the ground state energies in Ref. 19. The remarkable similarity to our quantum result for small N at the largest r_s is strong evidence for electron localization in that regime. For large N and r_s , however, our results differ from the classical ones in that we still have a weak remnant of shell effects.

Strong correlations can shuffle the energy ordering of different quantum states at fixed N . However, for $\omega > 0.01$, the ground state remains consistent with Hund’s first rule (except for $N = 3$). For smaller ω , we see a tendency toward violation of this rule, primarily for small N (which are in general more affected by strong correlations), as in the following example. For $N = 9$, the Hund’s rule ground state has $(L, S) = (0, 3/2)$. We find that for $\omega = 0.01$, the highly polarized state $(0, 7/2)$ becomes degenerate with the usual ground state (within our numerical accuracy). (All other (L, S) states lie higher in energy.) Note that $S = 7/2$ requires promotion between non-interacting shells, and so lies much higher in energy in the weakly interacting limit. At large r_s , this difference is overcome by the gain in interaction energy. The pair density g_T for both these $N = 9$ states is shown in Fig. 3. The more polarized state is clearly more localized; we find this is generally the case, as expected since exchange keeps the electrons apart.

In conclusion, we have investigated signatures of increasing electron-electron correlation in a parabolic circular quantum dot as the interaction strength increases. The scenario which emerges here is significantly different from the bulk:

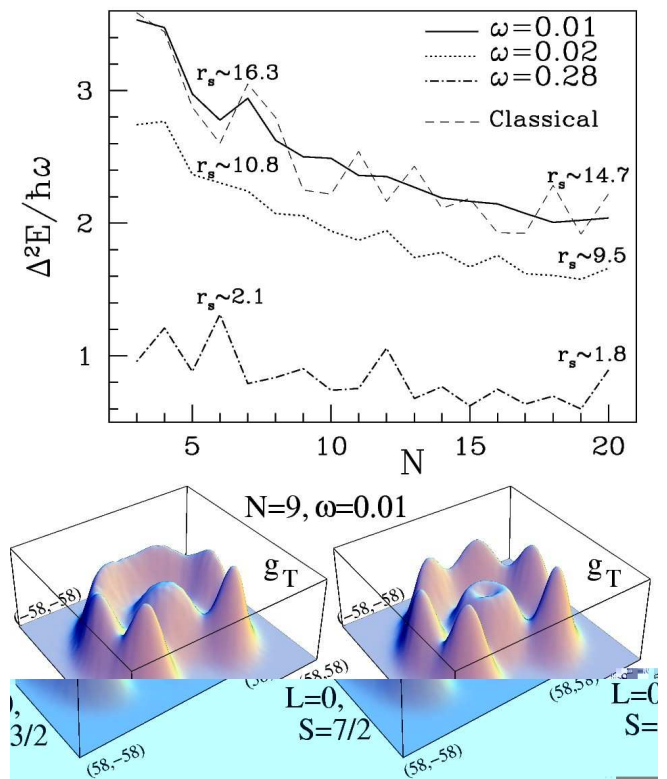


FIG. 3: Ground state energy. Top: Addition energy (normalized) as a function of N for three different ω and for the classical limit¹⁹ $r_s \rightarrow \infty$. As interactions strengthen because of decreasing ω , the mesoscopic fluctuations in $\Delta^2 E$ become weaker. Note that this happens more readily in the small N limit. Features in the $\omega = 0.01$ trace at small N are remarkably similar to those found in the classical limit, showing that electrons are nearly localized for small N . (The zero of the y-axis is offset for clarity, and the normalization of the classical trace is arbitrary.) Bottom: g_T for $N = 9$, $r_s \approx 15$ ($\omega = 0.01$), keeping an electron fixed on the outer ring ($\mathbf{r}_0 \approx (37, 0)$), for $L = 0$, $S = 3/2$ (left, the usual ground state) and $L = 0$, $S = 7/2$ (right). Increase of r_s , particularly for small N , often brings a strongly polarized state very close in energy to the “usual” ground state. In the case shown, the two states become essentially degenerate ($E = 1.464651H^*$) within statistical errors. The extent of Wigner localization is clearly stronger for the $S = 7/2$ state.

the cross-over between the delocalized and strongly inhomogeneous regimes appears to be completely smooth – there is no special value of r_s within our accessible range, $r_s < 18$. We stress that this goes beyond the expected finite-size rounding of a phase transition. Our main phenomenological findings are: Radial modulation appears directly in the electron density while observation of angular modulation requires, for all cases studied here, study of the pair density. Radial localization can be substantial for an r_s at which only weak incipient angular localization is visible. Increasing polarization significantly increases the amount of localization. Finally, there is a distinct tendency for small N dots to display stronger modulation.

Methods — As a starting point, we use the Kohn-Sham orbitals obtained from a density functional calculation done in

the local density approximation. We then perform a variational Monte Carlo (VMC) calculation using a trial wave function, Ψ_T , which is a linear combination of products of up- and down-spin Slater determinants of the Kohn-Sham orbitals multiplied by a Jastrow factor. The Jastrow factor effectively describes the dynamic correlation between the electrons coming from their mutual repulsion, whereas the near-degeneracy correlation is taken into account by having more than one determinant. We optimize the Jastrow parameters and determinant coefficients by minimizing the variance of the local energy.²¹ Finally, we use fixed-node diffusion Monte Carlo (DMC)^{6,22} to project the optimized many-body wave function onto a better approximation of the true ground state, an approximation that has the same nodes as Ψ_T .

The fixed-node DMC energy is an upper bound to the true energy and depends only on the nodes of the trial wave function obtained from VMC. We have calculated the energy $E(N, L, S)$ of a circular quantum dot for each N with angular momentum L and spin S – all good quantum numbers for our model. (S_z is also a good quantum number, and all our calculations are done for $S_z = S$; however, E is independent of S_z .) We investigated all possible combinations of L and S for the low lying states, and the combination yielding the lowest DMC energy, E_G , was taken as the ground state for that N .

For expectation values of operators that do not commute with the Hamiltonian – the density or the pair-density, for example – we use an extrapolated estimator^{6,23} (denoted F_{QMC} for an operator F) which eliminates the inaccuracy coming from the first-order error in the trial wave function. F_{QMC} is defined as $2F_{\text{DMC}} - F_{\text{VMC}}$ when $F_{\text{DMC}} \geq F_{\text{VMC}}$ and as $F_{\text{DMC}}^2/F_{\text{VMC}}$ otherwise.

In the multi-determinant expansion of Ψ_T , we keep only Slater determinants formed from the lowest energy Kohn-Sham orbitals for all of the results shown here. Our study is currently limited to $r_s \leq 18$ for technical reasons. The most serious is the failure of the VMC optimization as many Slater determinants need to be included for stronger interactions.

For two cases, corresponding to one moderate and one large r_s , we have done preliminary calculations with higher orbitals by including all determinants involving promotion of 2 electrons across a shell gap (10 configuration state functions for $N = 20$). This, then, allows for a change in the nodes of Ψ_T . We find that the change in the energy, as well as the change in density and pair-density, is small, though somewhat larger for greater r_s . Thus we believe that the fixed-node error in our calculations is under control.

Acknowledgments — This work was supported in part by the NSF (grants DMR-0506953 and DMR-0205328).

-
- ¹ G. Giuliani & G. Vignale, *Quantum Theory of the Electron Liquid* (Cambridge University Press, Cambridge UK, 2005).
- ² Tanatar, B. & Ceperley, D. M. Ground state of the two-dimensional electron gas. *Phys. Rev. B* **39**, 5005 (1989).
- ³ Attaccalite, C., Moroni, S., Gori-Giorgi P. & Bachelet, G. B. Correlation energy and spin polarization in the 2D electron gas. *Phys. Rev. Lett.* **88**, 256601 (2002); **91**, 109902(E) (2003).
- ⁴ Abrahams, E., Kravchenko, S. V. & Sarachik, M. P. Metallic behavior and related phenomena in two dimensions. *Rev. Mod. Phys.* **73**, 251 (2001).
- ⁵ Chakravarty, S., Kivelson, S., Nayak, C., & Voelker, K. Wigner glass, spin liquids, and the metal insulator transition. *Philos. Mag. B* **79**, 859 (1999); Jamei, R., Kivelson, S. & Spivak, B. Universal aspects of Coulomb-frustrated phase separation. *Phys. Rev. Lett.* **94**, 056805 (2005).
- ⁶ Foulkes, W. M. C., Mitas, L., Needs, R. J. & Rajagopal, G. Quantum Monte Carlo simulations of solids. *Rev. Mod. Phys.* **73**, 33 (2001).
- ⁷ Kouwenhoven, L. P., Austing, D. G. & Tarucha, S. Few-electron quantum dots. *Rep. Prog. Phys.* **64**, 701 (2001).
- ⁸ Reuter, D., et al. Coulomb-interaction-induced incomplete shell filling in the hole system of InAs quantum dots. *Phys. Rev. Lett.* **94**, 026808 (2005).
- ⁹ Reimann, S. M. & Manninen, M. Electronic structure of quantum dots. *Rev. Mod. Phys.* **74**, 1283 (2002)
- ¹⁰ Reusch B. & Grabert, H. Unrestricted Hartree-Fock for quantum dots. *Phys. Rev. B* **68**, 045309 (2003).
- ¹¹ Yannouleas, C. & Landman, U. Unified description of floppy and rigid rotating Wigner molecules formed in quantum dots. *Phys. Rev. B* **69**, 113306 (2004).
- ¹² Reimann, S. M., Koskinen, M. & Manninen, M. Formation of Wigner molecules in small quantum dots. *Phys. Rev. B* **62**, 8108 (2000).
- ¹³ Rontani, M., Cavazzoni, C., Bellucci, D., and Goldoni, G. Full configuration interaction approach to the few-electron problem in artificial atoms. Preprint, cond-mat/0508111 (2005).
- ¹⁴ Egger, R., Häusler, W., Mak, C. H. & Grabert, H. Crossover from Fermi liquid to Wigner molecule behavior in quantum dots. *Phys. Rev. Lett.* **82**, 3320 (1999); **83**, 462(E) (1999).
- ¹⁵ Filinov, A. V., Bonitz, M. & Lezovik, Yu. E. Wigner crystallization in mesoscopic 2D electron systems. *Phys. Rev. Lett.* **86**, 3851 (2001).
- ¹⁶ Pederiva, F., Umrigar, C. J. & Lipparini, E. Diffusion Monte Carlo study of circular quantum dots. *Phys. Rev. B* **62**, 8120 (2000); **68**, 089901(E) (2003).
- ¹⁷ Güçlü, A. D. & Umrigar, C. J. Maximum-density droplet to lower-density droplet transition in quantum dots. *Phys. Rev. B* **72**, 045309 (2005).
- ¹⁸ Ghosal, A., Umrigar, C. J., Jiang, H., Ullmo, D. & Baranger, H. U. Interaction effects in the mesoscopic regime: A quantum Monte Carlo study of irregular quantum dots. *Phys. Rev. B* **71**, 241306(R) (2005).
- ¹⁹ Bedanov, V. M. & Peeters, F. M. Ordering and phase transitions of charged particles in a classical finite two-dimensional system. *Phys. Rev. B* **49**, 2667 (1994).
- ²⁰ Koulakov, A. A. & Shklovskii, B. I. Charging spectrum and configurations of a Wigner crystal island. *Phys. Rev. B* **57**, 2352 (1998).
- ²¹ Umrigar, C. J., Wilson, K. G. & Wilkins, J. W. Optimized trial wave functions for quantum Monte Carlo calculations. *Phys. Rev. Lett.* **60**, 1719 (1988); Umrigar, C. J. in *Quantum Monte Carlo Methods in Physics and Chemistry*, edited by M. P. Nightingale and C. J. Umrigar (Kluwer, Dordrecht, 1999) pp. 129-160.
- ²² Umrigar, C. J., Nightingale, M. P. & Runge, K. J. A Diffusion Monte Carlo algorithm with very small time-step errors. *J. Chem. Phys.* **99**, 2865 (1993).

- ²³ Liu, K. S., Kalos, M. H. & Chester, G. V. Quantum hard spheres in a channel. *Phys. Rev. A.* **10**, 303 (1974).